Pergamon

*Int. J. Heat Mass Transfer.* Vol. 41, No. 12, pp. 1807–1820, 1998

Printed in Great Britain
0017–9310/98 $19.00+0.00

PII: S0017–9310(97)00238–X

# Fuel oil evaporation in swirling hot gas streams

BAIFANG ZUO and E. VAN DEN BULCK†

K.U. Leuven, Department of Mechanical Engineering, Celestijnenlaan 300A, B-3001 Leuven-Heverlee, Belgium

(*Received* 3 *December* 1996 *and in final form* 27 *July* 1997)

**Abstract**—As the limit on combustion generated pollutants is becoming more strict, a potentially ecological as well as economical new technology to decrease combustion generated pollutants by liquid fuel combustion is to adopt a fuel pre-vaporized, premixed combustion. This paper presents a study on the liquid fuel vaporizing and mixing processes. An effective method for the calculation of turbulent two phase evaporating flow has been developed, based on a realistic droplet vaporization model and a comprehensive turbulence–particle interaction model. Using the method, the influences of inlet gas swirling and heating on water droplets evaporation and mixing processes are numerically studied and compared with our experimentally measured data which show a reasonable agreement. Then, fuel droplets evaporation and mixing processes in the pre-vaporized, premixed oil burner at different confinement conditions are simulated. According to our studies, a strong inlet air swirl can greatly enhance mixing between the droplets, the air, and the recirculated flue gas which enters the burner. It also sharply reduces the droplet velocity, and thus prolongs the droplet vaporizing and mixing time to maintain a stable premixed combustion, proper combustion chamber confinement should be designed to ensure that sufficient recirculated flue gas is supplied to fully vaporize the fuel droplets before exiting from the burner and the actual mass fraction of the gaseous fuel is higher than the flammability limit one. 

## INTRODUCTION

As public interest in having ecologically-clean as well as economically sound power plants is growing, limit on combustion generated pollution is becoming more strict. But reducing harmful pollutants in the process of burning fossil fuel is a compromise: reducing carbon monoxide (CO) normally results in increased output of harmful $NO_x$, and vice versa [1]. It has been established that premixed natural gas burners offer good combustion efficiency and low pollutant emissions. Premixed oil burners, in which fuel oil is evaporated prior to combustion are now slowly entering the market in gas turbines as well as in household furnaces. But there are still some fundamental mechanisms facing the scaling up of such pre-vaporized, premixed oil burner which need to be studied [2, 3]. The main principle of this type of burner is to adopt a high inlet air swirl, thus inducing a strong in-furnace flue gas recirculation. These recirculated flue gases are then conducted into the burner (together with the inlet air) to evaporate the atomized fuel droplets (see Fig. 11). A lean combustible mixture is hence formed which leaves the burner and enters the premixed flame. At the exit of the burner the vortex breaks down, forming a recirculation zone which stabilizes the flame in free space, keeping combustion temperature and emissions low.

Thus, whether a fully premixed combustion can be achieved near the burner exit is mainly determined by the rate at which the fuel can evaporate and mix in combustible proportions with air. So a sound knowledge of the factors governing the rate of evaporation of fuel sprays is a key requisite to the success of such a pre-vaporized, premixed oil burner combustion. But in this two phase turbulent vaporizing process, there are strong couplings between the continuous and dispersed phases in both the mean and fluctuation levels. First, when a droplet travels in the continuous phase, it will exchange heat, mass, and momentum with the surrounding gas. Second, in turbulent flow condition when numerous droplets penetrate through the turbulent field of the continuous phase, they will exert some influence on the turbulent field, yielding some extra dissipation terms due to the particles slip velocity at the fluctuating level, the so called "turbulent modulation of continuous phase". At the same time, the particles themselves will experience certain dispersion due to the actions of the turbulent field, the so called "turbulent dispersion of dispersed phase".

On the iteration of particles and turbulent fluid flow, Rudinger [4] introduced a one-way coupling approach, which only considered the influence of gas to particles, while the gas flow field characteristics was assumed to be unaffected by the presence of particles. The one-way coupling approach has been used by many workers [5, 6], and is proper only for low particle mass loading. When the mass loading ratio is high, the coupling between the gas and the particles becomes two way [7, 8], where the particles act as sources of mass, momentum, and energy for the gas,

† Author to whom correspondence should be addressed.

## NOMENCLATURE

$A_r$ averaging parameter
$B_m$, $B_T$ Spalding mass and heat transfer numbers
$C_D$ drag coefficient
$C_{Pm}$ specific heat of the gaseous mixture at constant pressure [J kg$^{-1}$ K$^{-1}$]
$d$ droplet diameter [$\mu$m]
$F$ inter-phase diffusive transfer coefficient [kg m$^{-3}$ s$^{-1}$]
$F_T$, $F_m$ correction factor
$k$ continuous phase turbulent kinetic energy [m$^2$ s$^{-2}$]
$K_m$ thermal conductivity of the gaseous mixture [W m$^{-1}$ K$^{-1}$]
$Le$ Lewis number, $Le = K_m/(C_{pm}\Gamma_m)$
$L(T_s)$ latent heat of the vapor at temperature $T_s$ [J kg$^{-1}$]
$m_{ji}$, $\dot{m}$ inter-phase mass transfer rate [kg m$^{-3}$ s$^{-1}$]
$M$ mass flow rate [kg s$^{-1}$]
$Nu$ Nusselt number, $Nu = dh_H/K_m$
$Pr$ Prandtl number, $Pr = K_m/(\rho\nu_t C_{pm})$
$Q_L$ heat transferred into the droplet [W m$^{-3}$]
$r$ volume fraction
$r_s$ droplet radius [m]
$Re$ Reynolds number, $Re = V\mathrm{d}/\nu$
$S$ source term
$Sc$ Schmidt number, $Sc = \rho\nu_t/\Gamma_m$
$Sh$ Sherwood number, $Sh = h_m d/\Gamma_m$
$t_*$ droplet response time [s]
$T$ temperature [K]
$v'$ turbulent fluctuation velocity [m s$^{-1}$]
$V$ velocity [m s$^{-1}$]
$W$ molecular weight [kg mole$^{-1}$]
$Y$ mass concentration.

Greek symbols
$\Gamma$ diffusion coefficient [kg m$^{-1}$ s$^{-1}$]
$\delta$ film thickness [m]
$\varepsilon$ dissipation rate of turbulent kinetic energy [m$^2$ s$^{-3}$]
$\nu_p$ eddy viscosity of dispersed phase [m$^2$ s$^{-1}$]
$\nu_t$ eddy viscosity of continuous phase [m$^2$ s$^{-1}$]
$\rho$ density [kg m$^{-3}$]
$\tau$ Kolmogorov time scale [s]
$\tau_s$ characteristic time scale of large scale turbulent motion [s].

Subscripts
a air
F, f fuel oil vapor
g combustion product (flue gas)
m mixture of air and fuel vapor
p, 2 particle (droplet) phase
s droplet surface
t, 1 gaseous phase
0 initial status (also without the Stefan flow)
$\infty$ far from a droplet.

Superscripts and overscores
$\bar{}$ average value
* modified value.

and the gas controls the motion of particles. Basically, there are two approaches commonly used to predict particulate two-phase flow. One, called the Lagrangian approach, treats the particles as discrete entities in a turbulent flow field and their trajectories are calculated. The mutual coupling between fluid and particles is accounted for by estimating the particle source term for each computational cell visited by the particle. This is followed by a recalculation of the flow field incorporating these source terms. The other approach is the so-called Eulerian approach. In this approach, the cloud of particles is regarded as a continuum and the appropriate governing equations in differential form are solved for both phases. The effect of two-way coupling is incorporated as extra source terms in the continuum equations for both phases. Both approaches have been studied extensively and excellent reviews in both modeling schemes exist [7, 9].

Melville and Bray [10], and Michaelider [11] studied the influence of dispersed particles on the turbulence structure of the carrier phase. They employed the mixing length hypothesis to handle the gas–solid flow in free jets and fully-developed pipe flows. Their approach is limited to flows where turbulence structure changes at a slow rate in the main flow direction. Two different sets of empirical constants were required to achieve agreement with measurements in free jets and fully-developed pipe flow. More recently, general mathematical models for turbulent two-phase flows have been proposed by Chen and Wood [12] for Eulerian approach, and by Mostafa and Mongia [13] for Lagrangian approach. Both employed a two-equation $k$–$\varepsilon$ turbulent model. Their comparisons with measured data showed a reasonable agreement.

The theory of fuel droplet vaporization/combustion has been intensively developed during the past several decades. Detailed discussions on the subject may be found in the reviews of Sirignano [14–16], Faeth [17], Law [18], and Williams [19]. But these models are

based on many oversimplified assumptions, such as constant properties and unitary Lewis number in the gas phase near the droplet. The effect of the Stefan flow on heat and mass transfer between the moving droplet and the gas flow is assumed to be the same as in the case of the stagnant droplet. And the droplet surface is postulated to be at the normal boiling temperature. Recently, more comprehensive computational studies of the dynamics of a single vaporizing droplet inserted into a hot gas flow have been undertaken by several authors [20–22]. Renksizbulut and Yuen [20] presented the finite-difference analysis of flow and heat and mass transfer around the vaporizing heptane sphere including the effects of blowing and variable physical properties. Haywood and Renksizbulut [22] presented the finite-difference calculations of the life history of an *n*-heptane droplet moving and evaporating in its own super-heating vapor. Abramzon and Sirignano [23] employed a so-called film theory [24, 25] to account for the effect of the convective transport caused by the droplet motion relative to the gas. Consideration of variable thermophysical properties, non-unitary Lewis number in the gas film were also taken into account. As an illustration, the dynamic and vaporization histories of the droplets injected into the steady and fluctuating hot air streams were analyzed.

Based on the above analysis, the present study presents a comprehensive method for the calculation of turbulent two phase evaporating flow, which takes into account all the important effects influencing the droplet evaporation and mixing processes, such as variable physical properties and non-unitary Lewis number in the gas phase, influences of the gas phase temperature, the relative velocity between the droplet and the surrounding gas, the droplet diameter, and the Stefan flow on heat and mass transfer. A modified $k$–$\varepsilon$ turbulent model is used, with consideration of the turbulent particle dispersion and the particle turbulence modulation. As the rate of liquid droplet evaporation mainly depends on the surrounding gas temperature and the relative velocity between the droplet and the surrounding gas, the influences of inlet gas swirling and heating on the water droplets evaporation and mixing processes were studied numerically and experimentally.

Finally, the fuel droplets evaporation and mixing processes in the pre-vaporized, premixed oil burner at different confinement conditions were simulated to investigate the confinement influence of the combustion chamber on the fuel droplet evaporation and the premixed combustion processes. For this analysis, fuel oil is taken to be a single component liquid with properties as given in the appendix.

## THE MODELING OF TURBULENT EVAPORATING FLOW USING EULERIAN SCHEME

*Governing equations*

In Eulerian–Eulerian models, the equations describing the state of the phase are basically the Navier–Stokes ones, generalized so as to allow for the facts that each of the phase occupies only a part of the space, given by its volume fraction, and the phases are exchanging mass and properties. In addition, some assumptions are made that the dispersed phase is dilute and comprised of spherical mono-size droplets for which droplet–droplet interactions are negligible but fluid–droplet two-way interaction is allowed.

The steady state equations for the transport of volume fraction $r_i$ are then:

$$\nabla(\rho_i r_i \mathbf{V}_i) - \nabla(\Gamma_{r_i} \nabla r_i) = m_{ji} \tag{1}$$

where $m_{ji}$ is the inter-phase mass transfer rate from phase $j$ to phase $i$. $\Gamma_{r_i}$ is phase diffusion coefficient. Because both phases fill completely the available space, these volume fractions fulfill $r_1 + r_2 = 1$, at each point.

Conservation of any other variable $\Phi_i$ of phase $i$, can be expressed as:

$$\nabla(\rho_i r_i \Phi_i \mathbf{V}_i) - \nabla(\Phi_i \Gamma_{r_i} \nabla r_i) - \nabla(\Gamma_{\Phi_i} r_i \nabla \phi_i) = r_i S_{\Phi_i} + (F_{\Phi_i} + [m_{ji}])(\Phi_i^{\text{int}} - \Phi_i) \tag{2}$$

where $\Gamma_\Phi$ is an exchange coefficient, $S_\Phi$ is a source term, $F_\Phi$ is the inter-phase diffusive transfer coefficient, and $\Phi^{\text{int}}$ is the value of the property at the interface between the phases. The drag force, which appears in the momentum equations as the inter-phase diffusive transfer coefficient, has the form:

$$\mathbf{F}_{V_i} = \frac{3}{4} C_D \frac{\rho_1}{\Gamma_p} r_2 |\mathbf{V}_i - \mathbf{V}_j| (\mathbf{V}_i - \mathbf{V}_j) \tag{3}$$

where $\rho_1$ is the gaseous density, $r_2$ is the droplet volume fraction, and $C_D$ is the drag coefficient. As experimentally shown by Yuen and Chen [26], the drag coefficient of evaporating droplets may be well approximated by the 'standard drag curve' provided the gas viscosity and other physical properties are evaluated at the proper reference temperature and fuel concentration,

$$\bar{T} = T_s + A_r(T_\infty - T_s); \quad \bar{Y}_F = Y_{F_s} + A_r(Y_{F_\infty} - Y_{F_s}) \tag{4}$$

where $A_r$ is an averaging parameter, which is recommended to take the value of 1/3 ('1/3 rule').

*Two-phase turbulence model*

The hierarchy of turbulence closure models for single-phase flows range from simple zero-equation models to Reynolds-stress-transport models. The present modeling approach is based on the two-equation $k$–$\varepsilon$ turbulence model in which the turbulent stresses are modeled using a gradient constitutive equation. However, in two-phase flow, the continuous and the dispersed phase interact with each other at both the mean and fluctuation levels. At the fluctuation level, the droplets experience dispersion due to the action of the turbulence field while the turbulence

field itself experiences a modulation effect due to the presence of droplets. To model the droplet turbulent dispersion, the gradient type diffusion model for the dispersed phase turbulent fluxes is adopted,

$$\overline{v_i'v_j'} = -\frac{\nu_p}{2}\left(\frac{\partial V_i}{\partial x_j}+\frac{\partial V_j}{\partial x_i}\right)+\frac{2}{3}\delta_{ij}\left(\frac{1}{2}\overline{v_i'v_i'}+\nu_p\frac{\partial V_i}{\partial x_i}\right) \quad (5)$$

$$\overline{\rho_p'u_j'} = -\Gamma_t\frac{\partial\overline{\rho_p}}{\partial x_j};\quad \overline{\rho_p'v_j'} = -\Gamma_p\frac{\partial\overline{\rho_p}}{\partial x_j}. \quad (6)$$

The use of the Boussinesq assumption for the dispersed phase requires the definition of an 'effective' turbulent kinematic eddy viscosity $\nu_p$ and the turbulent diffusivity $\Gamma_t$ and $\Gamma_p$. These are determined from the characteristic analysis of the underlying turbulent motion by,

$$\frac{\nu_p}{\nu_t} = \frac{1}{1+t_*/\tau_s};\quad \Gamma_t = \frac{\nu_t}{Sc_t};\quad \Gamma_p = \frac{\nu_p}{Sc_p} \quad (7)$$

where $\tau_s$ is the characteristic timescale of large scale turbulent motion and is evaluated as $\tau_s = 0.125k/\varepsilon$; $t_*$ is the droplet response time and is evaluated as $t_* = \rho_p d_p^2/18\mu_t$. The turbulent Schmidt number is set to be $Sc_t = Sc_p = 0.7$, following the testing of Chen and Wood for axisymmetric flows.

Because the dispersed phase will also modulate the turbulence structure of the carrying gas flow, even with only a relatively small amount of droplets. This interaction between droplets and the continuous phase yields extra dissipation terms in the modeled equation for $k$ and $\varepsilon$, which is derived by including the inter-phase interaction force terms in the continuous phase,

$$\nabla(\rho_1 r_1 \mathbf{V}_1 k)-\nabla\left(\rho_1 r_1\frac{\nu_t}{\sigma_k}\nabla k\right) = \rho_1 r_1(P_k-\varepsilon)+\rho_1 r_1 S_k \quad (8)$$

$$\nabla(\rho_1 r_1 \mathbf{V}_1 \varepsilon)-\nabla\left(\rho_1 r_1\frac{\nu_t}{\sigma_\varepsilon}\nabla\varepsilon\right) = \rho_1 r_1\frac{\varepsilon}{k}(C_{1\varepsilon}P_k-C_{2\varepsilon}\varepsilon)+\rho_1 r_1 S_\varepsilon \quad (9)$$

where $P_k$ is the turbulent production term; $S_k$ and $S_\varepsilon$ are 'extra dissipation' terms due to the droplet slip velocity at the fluctuation level and, according to Chen and Wood, is a function of droplet response time,

$$S_k = -2\frac{k}{t_*}\frac{\rho_2 r_2}{\rho_1}[1-\exp(-0.5t_*\varepsilon/k)] \quad (10)$$

$$S_\varepsilon = -2\frac{\varepsilon}{t_*}\frac{\rho_2 r_2}{\rho_1}. \quad (11)$$

The model is valid for the situation $\tau_s > t_* \gg \tau$, where $\tau = \sqrt{\nu/\varepsilon}$ is the Kolmogorov timescale.

*Droplet vaporization model*

In the analysis of heat and mass transfer processes in the gas phase near the droplet surface, it is assumed that the gas phase heat and mass transfer may be considered as quasi-steady, and the thermophysical properties may be treated as constant, provided they are evaluated at some reference conditions (i.e. the '1/3 rule'). To take into account the effect of the convective transport caused by the droplet motion relative to the gas, the so-called 'film theory' is employed, which assumes that the resistance to heat or mass exchange between a droplet surface and the surrounding gas flow may be modeled by introducing the concept of a gas film of constant thickness: $\delta_t$ or $\delta_m$. From the requirement that the rates of a purely molecular transport by thermal conduction or diffusion through the film must be equal to the actual intensity of the convective heat or mass transfer between the surface and the external flow, the thickness of the thermal and diffusion films can be calculated as,

$$\delta_{T0} = \frac{2r_s}{Nu_0-2};\quad \delta_{m0} = \frac{2r_s}{Sh_0-2} \quad (12)$$

where $Nu_0$ and $Sh_0$ are the Nusselt and Sherwood number, respectively, $r_s$ is the droplet radius. However, for an evaporating droplet, the presence of the Stefan flow will influence the values of $\delta_T$ and $\delta_m$, since a surface blowing results in the thickening of the laminar boundary layer. This effect is considered by introducing a correction factor,

$$F_T = \delta_T/\delta_{T0};\quad F_m = \delta_m/\delta_{m0} \quad (13)$$

which represent the relative change of the film thickness due to the Stefan flow. Analytical results by Abramzon and Sirignano suggest that these factors could be approximated as a universal function of Spalding number,

$$F(B) = (1+B)^{0.7}\frac{\ln(1+B)}{B}. \quad (14)$$

Combining this extended film model, the classical expression for the instantaneous droplet vaporization rate then takes the form:

$$\dot{m} = 2\pi\bar{\rho}_m\bar{\Gamma}_m r_s Sh^*\ln(1+B_m) \quad (15)$$

$$\dot{m} = 2\pi\frac{\bar{K}_m}{\bar{C}_{pm}}r_s Nu^*\ln(1+B_T) \quad (16)$$

here $\bar{\rho}_m$, $\bar{K}_m$, $\bar{C}_{pm}$ are the averaged density, thermal conductivity, and the specific heat of the gas mixture in the film; $\bar{\Gamma}_m$ is the average binary diffusion coefficient of the vapor in the film; $Sh^*$ and $Nu^*$ are non-dimensional parameters which have the form,

$$Sh^* = 2+(Sh_0-2)/F_m;\quad Nu^* = 2+(Nu_0-2)/F_T \quad (17)$$

where $B_m$ and $B_T$ are the Spalding mass and heat transfer numbers, defined as,

$$B_m = \frac{Y_{F_s} - Y_{F_\infty}}{1 - Y_{F_s}}; \quad B_T = \frac{\bar{C}_{pm}(T_\infty - T_s)}{L(T_s) + Q_L/\dot{m}} \tag{18}$$

with $Y_F$ being the fuel mass fraction, $L(T_s)$ the latent heat of the vapor at temperature $T_s$, $Q_L$ the heat transferred from the gas phase to the droplet interior; subscript s and $\infty$ refer to the conditions near the droplet surface and external gas flow, respectively. When Lewis number is not unity, these two Spalding numbers are not equal, but related by the equation:

$$B_T = (1 + B_m)^\phi - 1; \quad \phi = \left(\frac{\bar{\Gamma}_m}{\bar{\Gamma}_t}\right)\left(\frac{Sh^*}{Nu^*}\right)\frac{1}{Le}. \tag{19}$$

The Nusselt and Sherwood numbers for non-vaporizing droplets is calculated using the Clift correlation [27]:

$$Nu_0 = 1 + (1 + Re\,Pr)^{1/3} f(Re)$$
$$Sh_0 = 1 + (1 + Re\,Sc)^{1/3} f(Re) \tag{20}$$

where $f(Re) = 1$ at $Re < 1$ and $f(Re) = Re^{0.077}$ at $Re < 400$.

The closure equation for the determination of interphase mass and heat transfer is the Clasius–Clapeyron correlation.

## STUDIES ON WATER SPRAY EVAPORATION

For a given fuel, the interfacial heat transfer between a fuel droplet and the surrounding gas is mainly influenced by the relative velocity between the droplet and the surrounding gas, the gas temperature, and the droplet diameter. Further, in the same fuel atomization conditions, the droplet vaporization time in a burner, defined as the total time needed for a droplet to be completely evaporated, is solely depended on the inlet gas swirling velocity and the inlet gas temperature. Thus, in the design of a prevaporized, premixed burner, whether fuel droplets can be completely evaporated and a fully premixed combustible gas mixture can be formed before leaving the burner exit will depend on the strength of the inlet gas swirl and the magnitude of the inlet gas temperature.

Experimental studies have been carried out on the full cone water spray evaporation. The experimental apparatus is shown in Fig. 1. Pure water is injected from the central nozzle with a feeding tube diameter of 16 mm. The injection pressure is kept at 7.2 bar with an initial spray velocity of 12.3 m s$^{-1}$. A co-flowing air stream is blown downwards through an annulus with a diameter of 50 mm. The swirl number of this co-flowing air stream can be changed by adjusting the mass flow ratio through the swirling conducted inlet air pipe and the no-swirling conducted inlet air pipe. The temperature of this co-flowing air stream is controlled by the heaters installed on the two inlet air pipes. Spray droplet velocities at different inlet gas temperatures and swirl numbers are measured by a 2-D Laser Doppler Velocimeter. The results are shown in Figs. 2–4.

Due to lack of direct means to measure the droplet evaporation rate here, numerical simulations [28] have also been carried out on this full cone water spray vaporization process. A variable grid of 42 axial nodes by 57 transverse nodes is used for this axi-symmetric flow calculation. At the inlet, the axial velocity of the inlet air is specified using a uniform profile with $V_{\text{lin}} = 4.7$ m s$^{-1}$. The swirl velocity is assumed a linear distribution along the radial direction, ranging from 8 m s$^{-1}$ to 25 m s$^{-1}$. The velocity of the dispersed phase is specified by subdividing the inlet region, each having a different injection angle, increasing from 0 to 15°. The initial droplet mean diameter is estimated to be 130 $\mu$, by comparison between the measured axial velocity distribution in the no swirl flow and other experimental data [29–31]. Turbulent kinetic energy is assumed to be 2% of the inlet mean kinetic energy. 3.5% of the characteristic length is used to evaluate the inlet dissipation. At the exit plane, the vanishing gradient boundary condition is imposed for all variables. While near the wall, the conventional wall function is used.

Figures 2 and 3 show the comparison of the droplet axial velocity distribution along the axis by numerical simulation and by experiments, in no swirl and swirl inlet air conditions, respectively. Good agreement is generally obtained. The relative higher measured velocities near the nozzle exit are expected because the numerical model does not consider the jet film breaking down process, and in the swirling flow they are further caused by the fact that only relative large droplets stay near the axis. Figure 4 gives further comparison of the droplet axial velocity profile along the radial direction at five different axial $Z$ positions, in the no swirl inlet air flow. Agreement is again satisfactory.

Figure 5 shows the calculated stream lines distribution in no swirl flow. At this condition, droplets are flowing and mixing with the co-flowing air only in a narrow region, and droplet axial velocity decreases slowly. As a result of poor mixing and low relative velocity difference, the interfacial heat transfer between the droplet and its surrounding gas is also low, which is shown in Fig. 6 where the gaseous temperature only slightly decreased from 352 K at inlet to 339 K near the base board. Thus droplet vaporization rate is low, as can be seen in Fig. 7 which shows that droplet mean diameter is decreased only from 130 $\mu$ at inlet to 115 $\mu$ near the base board.

In the swirl flow, however, strong swirl causes a reverse axial air flow near the nozzle exit, and a high radial gaseous velocity (see Fig. 8 which shows the stream lines distribution in swirl flow). As the initial droplet axial velocity is high, while radial velocity is low, intensive mixing and interfacial momentum, heat, and mass transfers between the droplet and its surrounding gas will take place. As a result, sharp drop of the droplet axial velocity and a quick increase of the

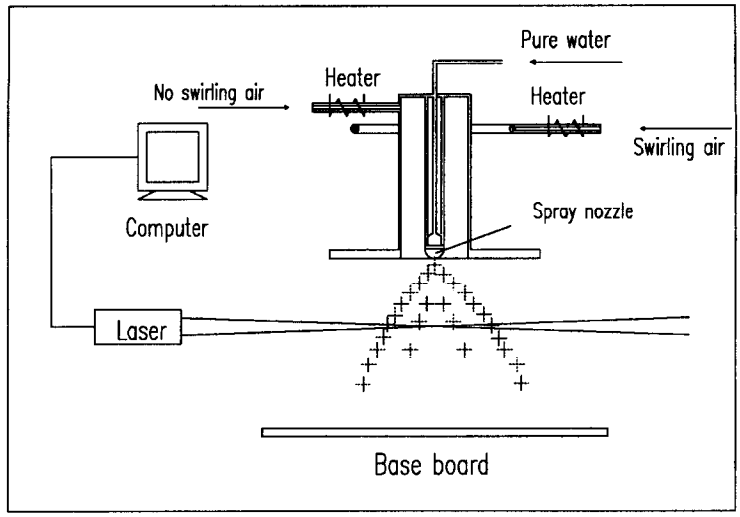


Fig. 1. Schematic diagram of the experiment apparatus.

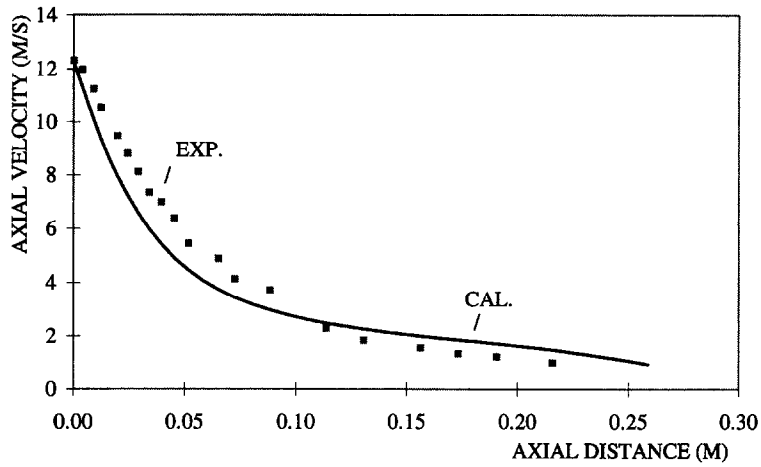


Fig. 2. Droplet axial velocity distribution along the axial line without swirl.

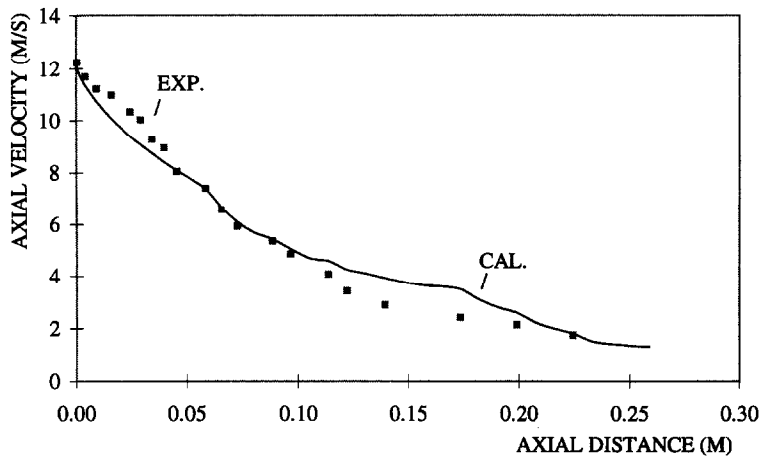


Fig. 3. Droplet axial velocity distribution along the axial line with swirl.

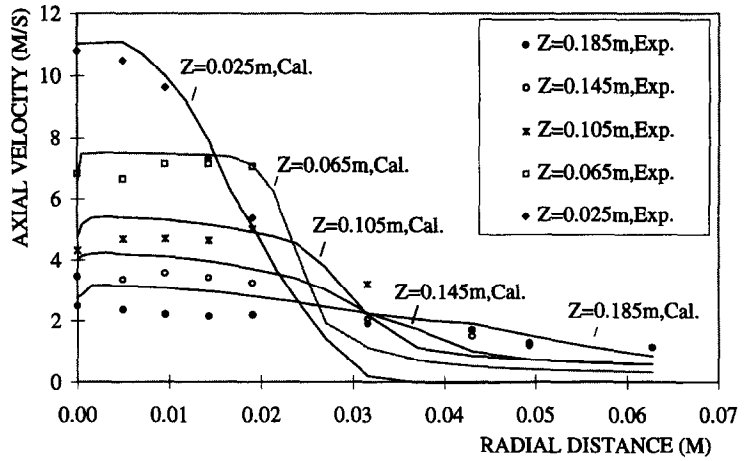


Fig. 4. Droplet axial velocity distributions along the radial distance without swirl.

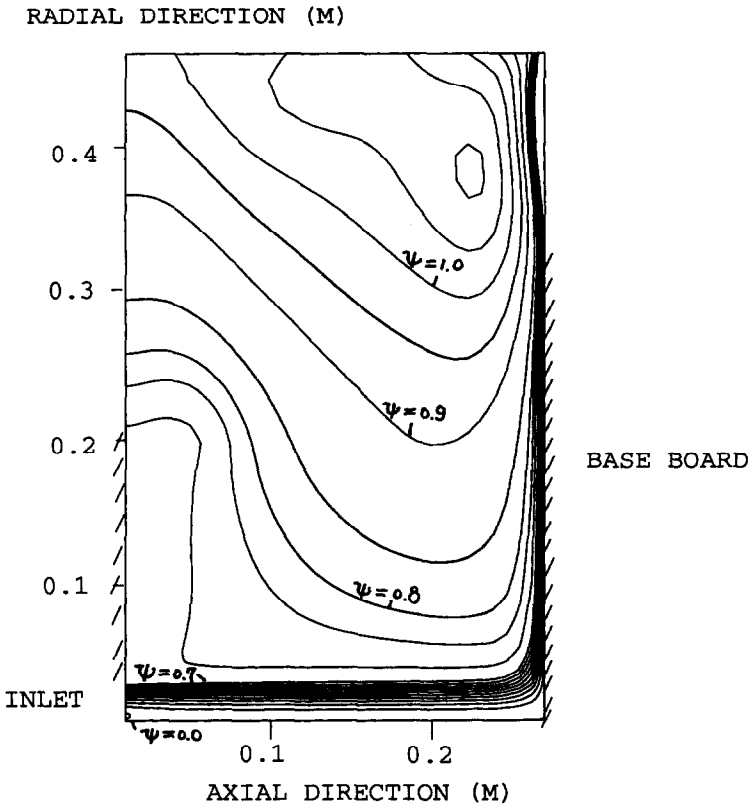


Fig. 5. Calculated stream lines distribution contour without swirl.

droplet radial velocity are observed. Thus the droplet evaporation time is prolonged, and turbulence intensity is strengthened. Figure 9 shows the calculated continuous phase temperature field, where gaseous temperature dropped from 327 K at inlet to 295 K near the base board, which is only marginally above the ambient temperature of 292 K. And droplet vaporization is faster, even though the inlet temperature at swirl flow is much lower than at no swirl condition, as can be seen in Fig. 10 which shows that the droplet mean diameter is decreased from 130 $\mu$ at inlet to 101 $\mu$ near the base board.

## NUMERICAL SIMULATIONS ON PREMIXED OIL BURNER EVAPORATION

As swirl can greatly enhance heat and mass transfer rates between the droplets and the surrounding gas,

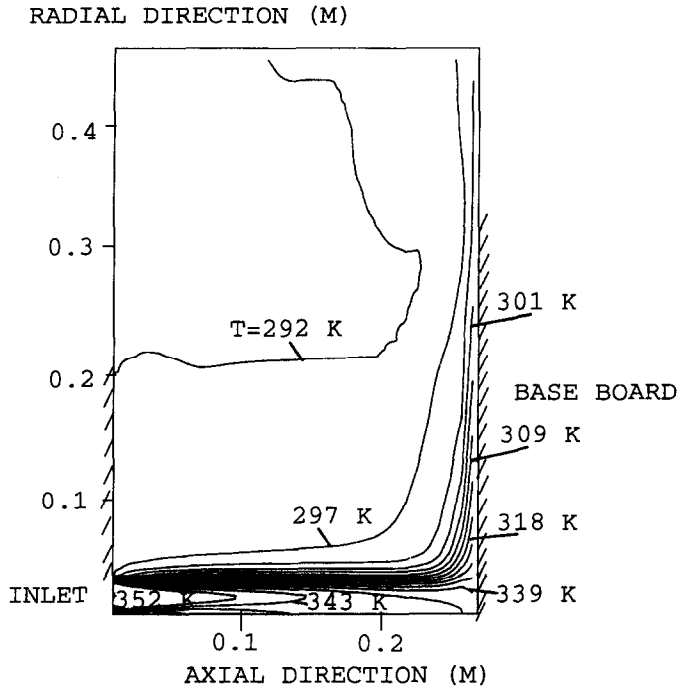


Fig. 6. Calculated gaseous temperature distribution contour without swirl.

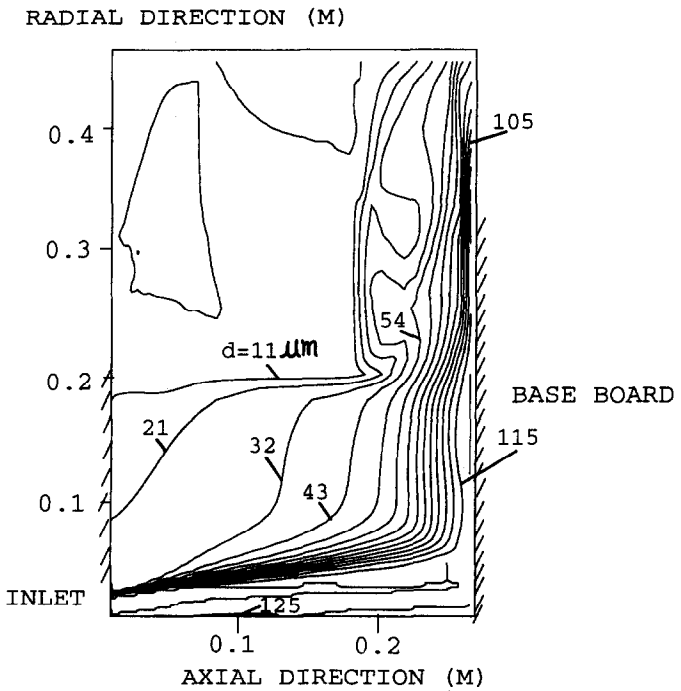


Fig. 7. Calculated droplet diameter distribution contour without swirl.

in the design of a pre-vaporized, premixed oil burner, inlet air enters the burner tangentially through the two slots near the burner wall to keep a maximum swirl number obtainable from the constraint of available fan capacity and mass flow rate of air. Thus, fuel droplets vaporization rate will now mainly depend on the other major factor: the available energy needed to evaporate the droplets, by increasing the temperature of the gaseous mixture. In the premixed oil burner-boiler system, this is achieved by introducing in-furnace flue gas recirculation into the burner. A schematic diagram of this premixed oil burner is

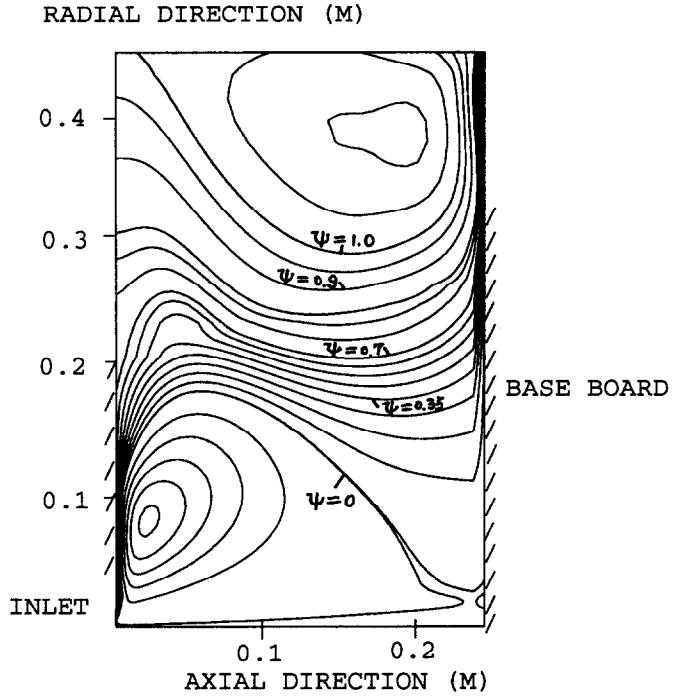


Fig. 8. Calculated stream lines distribution contour with swirl.

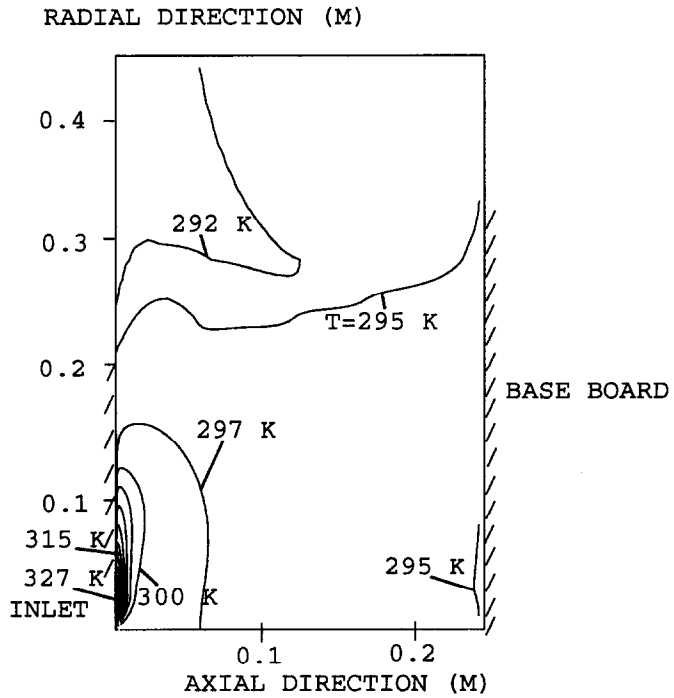


Fig. 9. Calculated gaseous temperature distribution contour with swirl.

shown in Fig. 11. The amount of the recirculated flue gas depends on the gas swirl number and on the combustion chamber confinement. The narrower the combustion chamber diameter and the exit area, the higher the amount of flue gas recirculation, which will result in a better fuel droplets vaporization and a lower NO emission level due to a higher flue gas dilution. For a 30 kW oil boiler with an initial fuel air equivalence ratio of about 0.8, studies [2, 3] show that the optimum chamber to burner diameter ratio

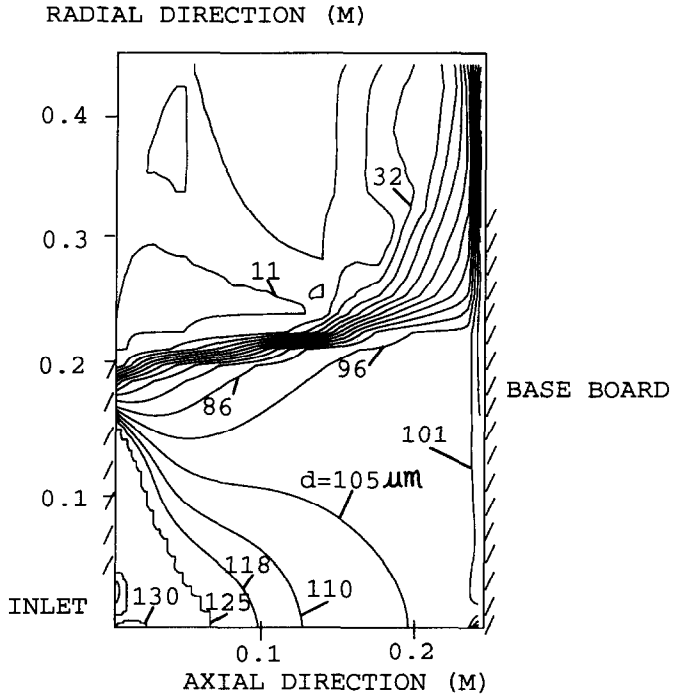


Fig. 10. Calculated droplet diameter distribution contour with swirl.

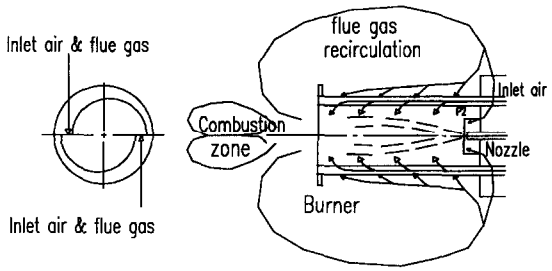


Fig. 11. Schematic diagram of the premixed oil burner.

is about 3 : 1. Increasing this diameter ratio to be above 5.4 : 1 will eventually quench the flame due to poor fuel droplets vaporization. While reducing this diameter ratio by a further 30% may result in a further 10% decrease of NO emission level, but the flame already reaches to its flammability limit. According to these studies, with a chamber to burner diameter ratio of 3 : 1, the recirculated flue gas pressure near the burner inlet port $P_2$ is about 15 N m$^{-2}$, with about 24% flue gas dilution and a stable premixed flame. But when the diameter ratio increases to 5.4 : 1, this pressure reduces to about 3 N m$^{-2}$, with about 5% flue gas dilution and the flame quickly quenches. How these changes in flue gas recirculation pressure will affect the fuel droplet vaporization process is numerically simulated here.

In the calculation, the recirculated flue gas temperature is estimated to be 900°C, according to our measurement. The inlet air and fuel temperatures are taken the same, 25°C. The mass flow rate of the fuel oil is 2.1 kg h$^{-1}$, and the excess oxygen concentration is 0.038. Initial oil spray injection velocity is 12.3 m s$^{-1}$, with an estimated mean diameter of 100 $\mu$m. Initial air injection velocity is estimated to be 17.3 m s$^{-1}$, which at continuous working condition enters the burner tangentially. As mentioned above, the inlet flue gas pressures are 15 and 3 N m$^{-2}$, respectively. Results are shown in Figs. 12–15.

Figure 12 shows the calculated gaseous temperature and gaseous velocity distributions at $P_2 = 15$ N m$^{-2}$. The inlet air is swirling into the burner through the slots near the burner wall. This strong swirl causes a low pressure zone near the burner axis, which will induce a small recirculation zone to be formed near the center of the burner exit useful to stabilize the premixed flame, and which will draw the recirculated flue gas into the burner through the burner inlet port. This high temperature flue gas then contacts directly with the injected fuel droplets. Thus the atomized fuel droplets are immediately surrounded by hot gas with a temperature of about 1000 K, and evaporated quickly. Figure 13 shows the calculated droplet diameter distribution. Near the burner exit, droplet diameter reduces to about 40% of its original value, which implies that about 93% of the liquid fuel has been evaporated. The remainder will be vaporized quickly as soon as they enter the recirculation zone near the burner exit by the hot combustion products. Thus a fully pre-vaporized, premixed combustible mixture is formed before entering the combustion zone.

But when the flue gas pressure near the burner inlet

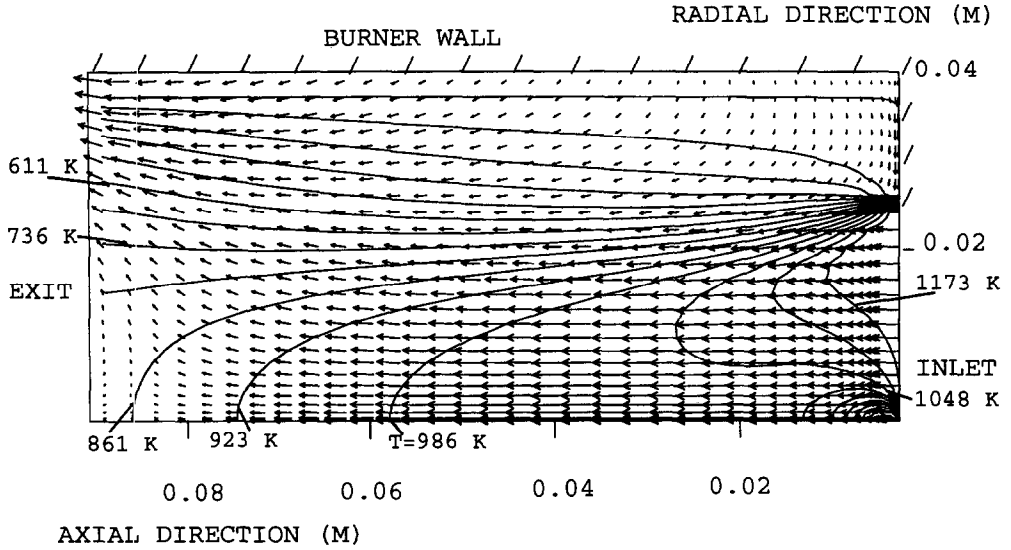


Fig. 12. Calculated gaseous velocity and temperature distribution ($P_2 = 15$ N m$^{-2}$).

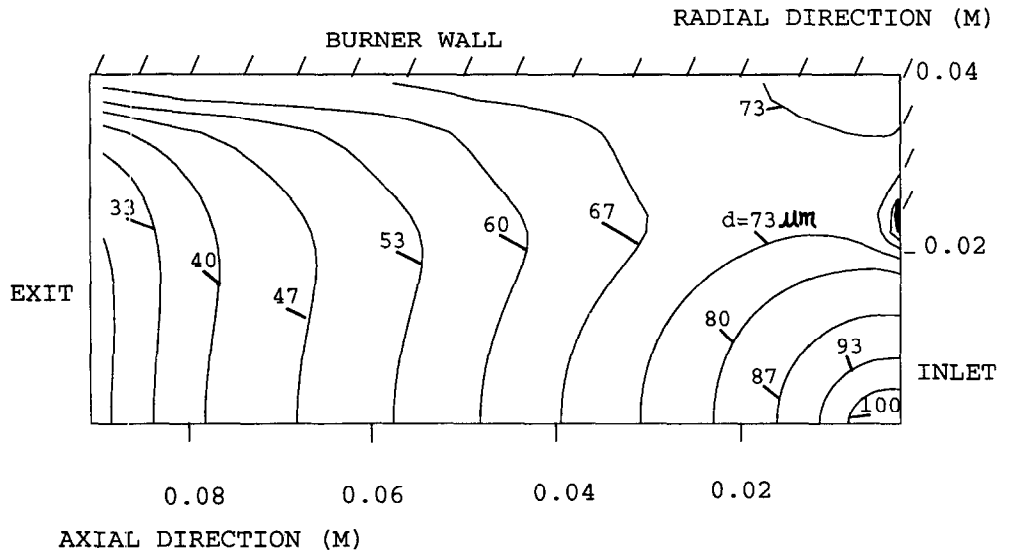


Fig. 13. Calculated droplet diameter distribution contour ($P_2 = 15$ N m$^{-2}$).

port drops to $P_2 = 3$ N m$^{-2}$, the percentage of the recirculated flue gas which enters the burner decreases to 5%, resulting in a lower inlet flue gas velocity at the burner inlet, and a much larger recirculation zone near the burner exit, as can be seen in Fig. 14. The figure also shows the calculated continuous phase temperature field. This time, the gaseous temperature decreases quickly from the inlet value of 1173 K to about 450 K near the burner exit. And the fuel droplets are also evaporated much slower, as is shown in Fig. 15. The exit mean droplet diameter remains as high as 71% of its original value, with only about 64% of the liquid fuel evaporated.

According to the detail kinetic analysis of the premixed oil laminar flame [32], the dilution flammability limit of evaporated fuel oil is approximately linearly increasing with the unburned mixture temperature. That is, in fuel lean condition, the flammability limit mass fraction of gaseous fuel is determined by,

$$\left(\frac{Y_f}{Y_{f=0}}\right)_{limit} = 1 - 0.00075T \tag{21}$$

where $Y_f$ is the mass fraction of gaseous fuel in the unburned mixture, $Y_{f=0}$ is the maximum mass fraction of gaseous fuel when the unburned mixture is not

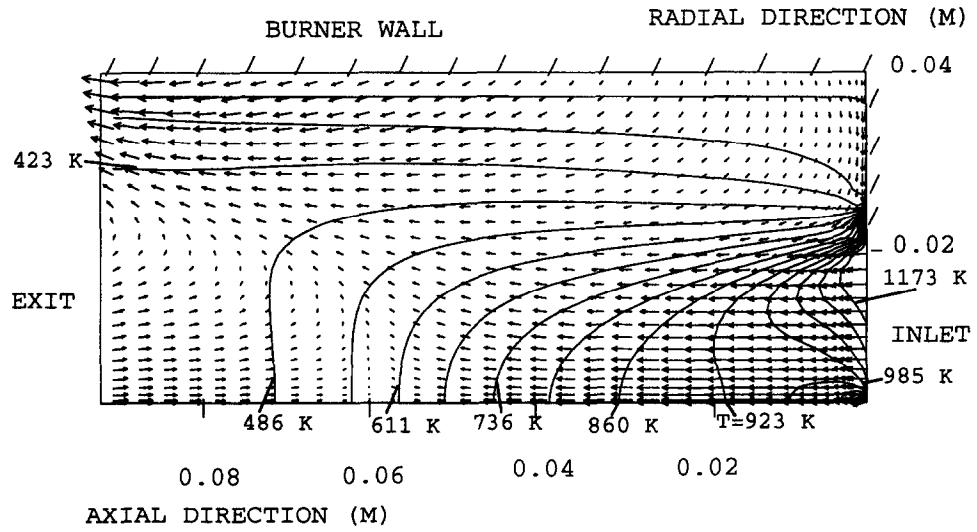


Fig. 14. Calculated gaseous velocity and temperature distribution ($P_2 = 3$ N m$^{-2}$).

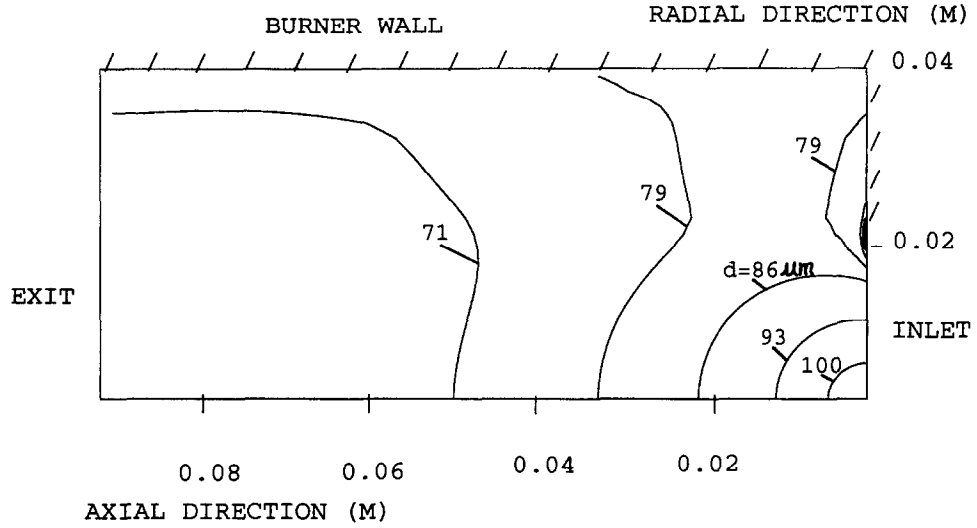


Fig. 15. Calculated droplet diameter distribution contour ($P_2 = 3$ N m$^{-2}$).

diluted by flue gas and fuel droplets are fully evaporated, $T$ is the unburned mixture temperature in Kelvin. While the actual mass fraction of gaseous fuel in the unburned mixture can be estimated by

$$\left(\frac{Y_f}{Y_{f=0}}\right)_{act} = \left(1-\frac{M_g/W_g}{M_g/W_g+M_a/W_a+M_f/W_f}\right)\left[1-\left(\frac{d}{d_0}\right)^3\right] \quad (22)$$

where $M_a$, $M_f$, $M_g$ are mass flow rates of air, fuel, and flue gas which enters the burner. $W_a$, $W_f$, $W_g$ are their molecular weights, respectively. $d/d_0$ is the ratio of the exit droplet diameter to its initial value (un-evaporated). When the flue gas pressure near the burner inlet port equals 15 N m$^{-2}$, the actual and the flammability limit mass fraction ratio of gaseous fuel near the burner exit are 0.674 and 0.542, respectively. So the actual value is higher than the flammability limit one, a stable premixed flame is expected. But when the flue gas pressure near the burner inlet port reduce to 3 N m$^{-2}$, the calculated actual and flammability limit mass fraction ratio of gaseous fuel near the burner exit are 0.507 and 0.625, respectively. As the actual value now is lower than the flammability limit one, a premixed flame can no longer sustain. And the high swirl flow will eventually quench the flame, as has been observed.

## CONCLUSION

A comprehensive method for two phase evap-

orating flow calculation has been developed. This model takes into account all the important effects which influence the droplet evaporation and mixing processes, such as variable physical properties and non-unitary Lewis number in the gas phase, influences of the gas phase temperature, the relative velocity between the droplet and the surrounding gas, the droplet diameter, and the Stefan flow on heat and mass transfer. A modified $k$–$\varepsilon$ turbulent model is used, with consideration of the turbulent particle dispersion and the particle turbulence modulation. Good agreements with the measured data with and without swirl prove the method having a reasonable prediction accuracy.

In the design of a pre-vaporized, premixed oil burner, two major factors control the evaporation and mixing processes of the atomized fuel droplets: the inlet air swirl and the in-furnace flue gas recirculation. A strong inlet air swirl can greatly enhance mixing between the droplets, the air, an the recirculated flue gas which enters the burner. It also sharply reduces the droplet axial velocity, and thus prolongs the droplet evaporation and mixing time.

In-furnace flue gas recirculation is the main way to supply energy for fuel droplets evaporation. To maintain a stable premixed combustion, proper combustion chamber confinement should be designed to ensure that sufficient recirculated flue gas is supplied to fully vaporize the fuel droplets before exiting from the burner and the actual mass fraction of the gaseous fuel is higher than the flammability limit one.

## REFERENCES


1. Zuo, B.-F., Ngendakamana, Ph. and Hore, F., Pollutant generation by combustion of oil boilers. *Bull. Soc. Chim. Belg.*, 1992, **101,** 859–869.
2. Zuo, B.-F. and Van den Bulck, E., A Reynolds stress, strained flamelet modeling of swirling turbulent premixed combustion, submitted for publication in *Combustion Theory and Modelling*, 1997.
3. Zuo, B.-F. and Van den Bulck, E., Numerical study of the influence of confinement and fuel air ratio on $NO_x$ emission of pre-vaporized, premixed oil burner combustion. Joint meeting of the French and Belgian sections of the Combustion Institute, Villeneuve d'Ascq, France, 27–30 May 1997.
4. Rudinger, C., Some effects of finite particle volume on the dynamics of gas-particle mixture. *AIAA Journal*, 1965, **3,** 1217–1222.
5. Batchelor, G. K., Transport properties of two phase materials with random structure. *Ann. Rev. Fluid Mech.*, 1974, **6,** 227–255.
6. Boysan, F. and Swithenbank, J., Spray evaporation in recirculating flow. *Seventeenth Symposium (International) on Combustion*. The Combustion Institute, 1979, pp. 443–454.
7. Crow, C. T., Review—numerical methods for dilute gas-particle flows. *J. Fluids Engng*, 1982, **104,** 297–303.
8. DiGiacinto, M., Sabetta, F. and Piva, R., Two-way coupling effects in dilute gas-particle flows. *ASME Paper* 82-*WA/FE*-1, 1982.
9. Faeth, G. M., Recent advances in modeling particle transport properties and dispersion in turbulent flow. *Proceedings of ASME–JSME Therm. Engng Conf.*, Vol. 2. ASME, pp. 517–534.
10. Melville, W. K. and Bray, K. N. C., A model of the two-phase turbulent jet. *International Journal of Heat and Mass Transfer*, 1979, **22,** 647–656.
11. Michaelides, E. E. A model for the flow of solid particles in gases. *International Journal of Multiphase Flow*, 1984, **10,** 61–77.
12. Chen, C. P. and Wood, P. E., A turbulence closure model for dilute gas particle flows. *Can. J. Chem. Engng*, 1985, **63,** 349–360.
13. Mostafa, A. A. and Mongia, H. C., On the interaction of particles and turbulent fluid flow. *International Journal of Heat and Mass Transfer*, 1988, **31,** 2063–2075.
14. Sirignano, A., An integrated approach to spray combustion model development. *Combust. Sci. Technol.*, 1988, **58,** 231–251.
15. Sirignano, W. A., The formulation of spray combustion models resolution compared to droplet spacing. *Journal of Heat Transfer*, 1986, **108**(3), 633.
16. Sirignano, W. A., Spray combustion simulation. In *Numerical Simulation of Combustion Phenomena*, ed. R. Glowinski, B. Larrouturou and R. Teman. Springer, Heidelberg, 1985.
17. Faeth, G. M., Current status of droplet and liquid combustion. *Prog. Energy Combust. Sci.*, 1977, **3,** 191–224.
18. Law, C. K., Recent advances in droplet vaporization and combustion. *Prog. Energy Combust. Sci.*, 1982, **8,** 171–201.
19. Williams, A., *Combustion of Sprays of Liquid Fuels*. Elek Science, London, 1976.
20. Renksizbulut, M. and Yuen, M. C., Numerical study of droplet evaporation in a high-temperature stream. *Journal of Heat Transfer*, 1983, **105,** 389–397.
21. Patnaik, G., Sirignano, W. A., Dwyer, H. A. and Sanders, B. R., A numerical technique for the solution of a vaporizing fuel droplet, dynamics of reaction systems. *Prog. Astronaut. Aeronaut.*, 1986, **105,** 253–264.
22. Haywood, R. and Renksizbulut, M., On variable properties, blowing and transient effects in convective droplet evaporation with internal circulation. *Proceedings of Eighth Int. Heat Transfer Conf.*, Vol. 4. San Francisco, 1986, pp. 1861–1866.
23. Abramzon, B. and Sirignano, W. A., Droplet vaporization model for spray combustion calculations. *International Journal of Heat and Mass Transfer*, 1989, **32,** 1605–1618.
24. Bird, R. B., Stewart, W. E. and Lightfoot, E. N., *Transport Phenomena*. Wiley, New York, 1960.
25. Frank-Kamenestskii, D. A., *Diffusion of Heat Transfer in Chemical Kinetics*, 2nd edn. Plenum Press, New York, 1969.
26. Yuen, M. C. and Chen, L. W., On drag of evaporating liquid droplets. *Combust. Sci. Technol.*, 1976, **14,** 147–154.
27. Clift, R., Grace, J. R. and Weber, M. E., *Bubbles, Drops and Particles*. Academic Press, New York, 1978.
28. Zuo, B.-F. and Van den Bulck, E., Computation of turbulent evaporating sprays injected into swirling hot gas streams. 2nd PHOENICS Dutch Users Conference, Leuven, 1996.
29. Ricou, F. P. and Spalding, D. B., Measurement of entrainment by axisymmetrical turbulent jets. *Journal of Fluid Mechanics*, 1961, **11,** 21–32.
30. Lefebvre, A. H., Fuel atomization, droplet evaporation, and spray combustion. In *Fossil Fuel Combustion*, ed. W. Bartok and A. F. Sarofim, Chap. 9. John Wiley and Sons, New York, 1991.
31. Schetz, J. A., Injection and mixing in turbulent flow. In *Progress in Astronautics and Aeronautics*, ed. M. Summerfield, Vol. 68. AIAA, New York, 1980.
32. Zuo, B.-F. and Van den Bulck, E., A quasi-global mechanism for oxidation of fuel oil and the laminar flame data library. *Combustion and Flame*, in press.

## APPENDIX: FUEL OIL PHYSICAL PROPERTIES

Physical properties of fuel oil vapor/air mixture were calculated at reference film conditions (the '1/3' rule) using the standard additive rules for an idea gas

$$\bar{\rho}_m = [(\bar{Y}_F/\rho_F)+(1-\bar{Y}_F)/\rho_a]^{-1}$$

$$\bar{C}_{pm} = C_{pF}\bar{Y}_F + C_{pa}(1-\bar{Y}).$$

The Wilke rule was used for the dynamic viscosity and thermal conductivity. In the analysis fuel oil is taken to be a single component liquid with the following correlation being used:

binary diffusion coefficient:

$$\Gamma_m = 5.46\times10^{-6}(T/300)^{1.583}P^{-1} \quad [m^2\ s^{-1}]$$

vapor thermal conductivity:

$$k_F = 1.213\times10^{-5}(T/300)^{1.8} \quad [kJ\ m^{-1}\ s^{-1}\ K^{-1}]$$

vapor dynamic viscosity:

$$\mu_F = [0.04+1.75(T/1000)]\times10^{-5} \quad [kg\ m^{-1}\ s^{-1}]$$

vapor specific heat:

$$C_{pF} = 0.1066+5.761(T/1000)-1.674(T/1000)^2 +0.473(T/1000)^3 \quad [kJ\ kg^{-1}\ K^{-1}].$$

Liquid fuel oil properties (except viscosity) were assumed to be constant and evaluated at some average temperature

$$\bar{T}_2 = 0.5[T_0+T_s]$$

where $T_s$ is the droplet surface temperature. Thus, for example, at $\bar{T} = 400$ K

$$\rho_2 = 810\ kg\ m^{-3}$$

$$C_{p2} = 2.2\ kJ\ kg^{-1}\ K^{-1}$$

$$k_2 = 1.054\times10^{-4}\ kJ\ m^{-1}\ K^{-1}$$

$$L(\bar{T}_2) = 270\ kJ\ kg^{-1}.$$

The liquid dynamic viscosity was calculated at the surface temperature using the following approximation:

$$\mu_2 = 1.4\times10^{-3}\exp(T_s/300-1) \quad [kg\ m^{-1}\ s^{-1}].$$

The average molecular weight is 170, and the average boiling temperature is 523 K at atmospheric pressure.